Steering and *In-situ* Monitoring of Drying Phenomena during Film Fabrication

Fabian Scheepers,[1] Andrea Stähler,[1] Markus Stähler,[1] Marcelo Carmo,[1] Werner Lehnert[1,2] and Detlef Stolten[1,3]

[1] Forschungszentrum Jülich GmbH, Institute of Energy and Climate Research (IEK-3): Electrochemical Process Engineering, 52425 Jülich, Germany

[2] Modeling in Electrochemical Process Engineering, RWTH Aachen University, Germany

[3] Chair for Fuel Cells, RWTH Aachen University, Germany

Corresponding author: Fabian Scheepers, mail: f.scheepers@fz-juelich.de, tel: +49 2461 61-2177,
ORCID: 0000-0001-6243-4291

Abstract

During film fabrication, the phenomena of crack formation and delamination are often observed, dramatically hindering the discovery and characterization of new materials for energy applications. In this work, we report on a novel approach to fully steer the drying parameters or "knobs" that are commonly used during electrode manufacture. It allows us to precisely *in-situ* control and monitor the solvent-specific evaporation rates that affect the development of suspension composition during drying. We managed to control the capillary stress inside the layer by precisely controlling the selectivity of solvent evaporation. Large cracks result when the surface tension increases over time and layer delamination occurs. When using an n-propanol/water system, critical crack formation is achieved when water is enriched by decreasing the gas exchange during drying or preloading the gas phase with water vapor. High gas exchange rates inhibit the water's enrichment and therefore only small surface cracks develop. The experiments also surprisingly indicate that the drying temperature has no significant effect on crack formation. These results are of fundamental meaning for the future development of electrodes as the drying step has a high impact on the products specification and now can be ultimately controlled. The future development of electrodes will surely benefit from this achievement in the controlled fabrication of films for a variety of applications.

Keywords

Electrode Fabrication, Crack Formation, Surface Tension, Drying Mechanisms, Slot Die Coating

Introduction

Today, a variety of methods are used to fabricate thin films composed of powdery materials, such as automated ultrasonic spraying [1], spin-coating [2], ink-jet printing [2], screen printing [3], dip coating [4], gravure coating [5], slot-die coating [6], blade coating [7] and others. However, during the drying step of a wet thin-film, for all of the methods described above, the often described phenomena of "crack formation" [8], delamination [9], Rayleigh-Bénard-[10] and Marangoni-convection [11] are often observed. It is indispensable to obtain control over these mechanisms during film fabrication so that specific properties, such as homogeneity [12], agglomeration [13], porosity [14], hydrophilicity/hydrophobicity [15], roughness [16] and adhesion [9] can be precisely tuned.

In various sectors, the concepts of thermodynamics and hydrodynamics are already applied to film drying, for example in photovoltaic [17], battery [18] and pharmaceutical contexts [19]. In particular, liquid phases consisting of multiple solvents allow the steering of the drying process, as heat and substance-specific mass transfer can be regulated in a desired direction by adjusting the drying conditions. The corresponding parameters are the drying temperature [20], gas exchange rate [21] and gas humidity [21]. Here, we use these mechanisms to macroscopically steer the film formation process, in particular the formation of cracks over the surface area, inside its macroscopic structure and at the interface with the coated substrate. During the drying of a film, the particle-particle distances decrease due to the evaporation of solvent between non-volatile particles. After certain time, particles collide and capillary pressure will result in cohesive interaction between them caused by liquid menisci between the particles [22]. By further shrinkage of the film, a pore network is formed that is under capillary pressure resulting from the surface tension of the liquid on the top surface [23]. The emptying of the liquid filled pores starts for large pores by which wiping out the cohesion between the affected particles while particles forming small pores are still in interaction. Simultaneously, air starts to penetrate the particle network [24]. The continuing shrinkage of the layer thus results in cracks between already emptied pores [8]. The effect begins at the surface and propagates in the direction of the substrate [25]. It was shown that the particle size [26] and surface tension affect the crack behavior [27], as well as larger particle size distribution and fissured particle surface increasing the maximum stress development [28]. Additionally, the tendency of cracking increases when the film thickness becomes larger; however, the drying speed seems to have no influence on this behavior [29]. At the interface between film particles and substrate, cracking is known as film delamination. The film however can possibly withstand delamination depending on how strong is the additional contribution from adhesion between film particles and substrate [30]. With respect to the drying conditions, it was found that an increase in the drying temperature correlates with a higher crack ratio of the surface [25]. In contrast, drying under humidified air seems to inhibit the cracking tendency [31].

With regard to the formation of cracks in fuel cell electrodes, an analysis of how they can affect the performance and durability of the electrodes is in progress [32]. While electrical contact could be inhibited, fluid transport can be enhanced through the presence of cracks. There is, however, no clear evidence to show both the positive or negative effects; and cracks are generally prevented in order to comply with good homogeneity of the film as a means of performing visual quality control [32]. For this system, the literature shows that high mixing time of the dispersion and low drying rates, leading to crack-free electrodes [33]. Another possibility for preventing cracks is based on a change in the chemical composition of the suspension. Less crack formation was observed when the viscosity of the dispersion was increased by the use of additives [34]. Furthermore, higher ionomer-to-solids ratios reduce the generation of cracks, as well as when water-based dispersions are used [35]. Previous studies have investigated the use of various solvents and note that crack formation behavior was particularly associated with the solvents [36] as well as with solvent mixture composition and film thickness [37]. It should be noted that these studies were based on random changes of the suspension mixing procedure/composition; in other words, by simply following a “trial and error” approach. The issue here is that different physiochemical and mechanical properties, such as dispersion viscosity, film elasticity and particle arrangement and interactions, are obtained. In consequence, up until now the crack formation, for instance, was not correlated to suspension properties and drying conditions, seriously hindering further breakthroughs in electrode fabrication R&D.

In this work, a novel *in-situ* approach is used that is a powerful tool for future investigation and advanced analysis of film/electrode manufacturing. The capillary stress leading to crack formation strongly depends

on the drying conditions as it correlates to the composition of the suspension as a function of time. Utilizing selective evaporation, the capillary stress inside a catalyst layer was controlled (reduced or increased), allowing for ultimate manipulation in designing novel electrode structures. All fabricated structures obtained here from different solvent mixtures can be tuned by merely changing the drying parameters.

Experimental

Principle

Figure 1 shows the measurement methods as well as the dispersions that were used to generate layers. The dispersions consist of perfluorosulfonic acid polymer (Nafion) and carbon black (XC-72R). As liquid phase mixtures of water and propanol were used. The real-time suspension composition of the film during drying is plotted by means of an *in-situ* FTIR spectrometer, coupled to the drying step.

Slot Die Coating

The suspensions were applied with a single-layer slot die (TSE Troller AG) to a glass fiber-reinforced polytetrafluorethylene (PTFE) substrate (120 µm). The substrate was vacuum-fixed to a movable table (TableCoater, TSE Troller AG). The table velocity was 0.9 m min^{-1} and the dosing rate was 7.5 ml min^{-1}. At a coated width of 50 mm, the wet film thickness was about 167 µm. The length is generally variable, with 70 mm chosen for these experiments. A more detailed description of the setup has already been published [38].

Drying Test Station

The transfer of the coated PTFE substrate from the slot die to the drying test station was automated, guaranteeing high reproducibility. The layers generated were dried under controlled conditions and were laminar overflowed with nitrogen (5.0, Air Liquid) at a defined volume flow, leading to a loading of the gas with solvent. The heating of the substrate commenced immediately after closing the drying chamber, causing increasing drying rates over time until the set temperature was reached. However, the nitrogen gas flow was already preheated to the target temperature. A pre-wetting of the nitrogen was possible through a continuous metering and evaporation of water by means of a syringe pump (KDS100, KD Scientific), generating the desired water vapor pressure. After overflowing the wet layer, the loaded gas was transported to an FTIR-spectrometer (FTIR-S)(CX4000, Gasmet), which indirectly determined the mean drying rate of the entire layer by means of a software evaluation of the gas phase composition (Calcmet v12.16, Gasmet). The total mass of the remaining solvent in the drying layer is the integral of the drying rates of the solvents over time when assuming the layer to be dry at the end of the process. This assumption proved to be valid within the uncertainty of the measuring principle itself. As the mass fractions of the solids are known from dispersion preparation, the composition of the entire layer is re-calculable as a function of time. A detailed description of the drying test station and its measuring principle, error calculation and validation was previously published in a separate paper [39]. All dried layers were then observed by a stereomicroscope (Stemi 2000-C with AxioCam ICc3, Zeiss).

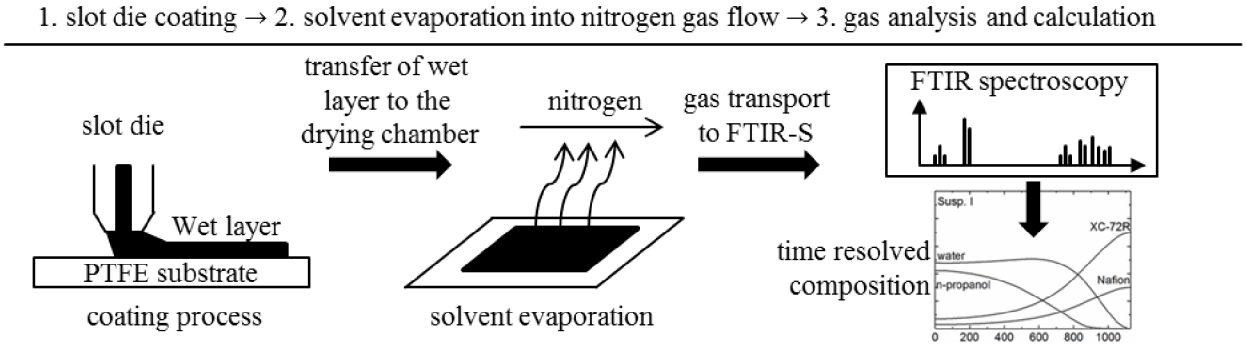

Suspension	I	II	III	IV	V
n-propanol (wt%)	43	48	53	58	63
Water (wt%)	47	42	37	32	27
Carbon black (wt%)	7	7	7	7	7
Nafion® (wt%)	3	3	3	3	3

Figure 1. The slot die and drying test station are schematically illustrated. The table coater is automatically moved to the drying chamber after the coating process. The film is purged with nitrogen. The dispersion and liquid compositions are then calculated from the gas phase composition and detected by an FTIR-spectrometer. The attached table shows the mass fractions of carbon black dispersions used for the experiments.

Results and Discussion

Variation of Suspension Composition/Concentration

All samples in this section were measured under the same drying conditions. The gas temperature, as well as the substrate temperature, was set to T = 40 °C and the layer was overflowed with dry nitrogen (water partial pressure $p_w = 0$ Pa) at a gas flow velocity of 4.4 mm s^{-1}. These parameters remained as the reference condition of this work.

The drying curves and structure formation resulting from these experiments are shown in Figure 2. When drying leads to an enrichment of water in the liquid phase (see the drying of Suspension I and II), the surface tension will increase over time; thus, the capillary force in the layer will notably increase, leading to both delamination and large cracks according to the Griffith-criterion (see Case 1) [8]. In contrast, if n-propanol is enriched (compare the drying of Suspension IV and V), the surface tension will drop, reducing the capillary stress in the layer. Additionally, the adhesion force is stronger than the attraction between the particles. Small surface cracks and no delamination results from this case (Case 3). Case 2 describes a transition area that results when the solvent drying is quasi-azeotropic, meaning that no depletion of either n-propanol or water occurs. Because of the local enrichment of water, many small cracks occur; however, large cracks, as well as delamination, are prevented.

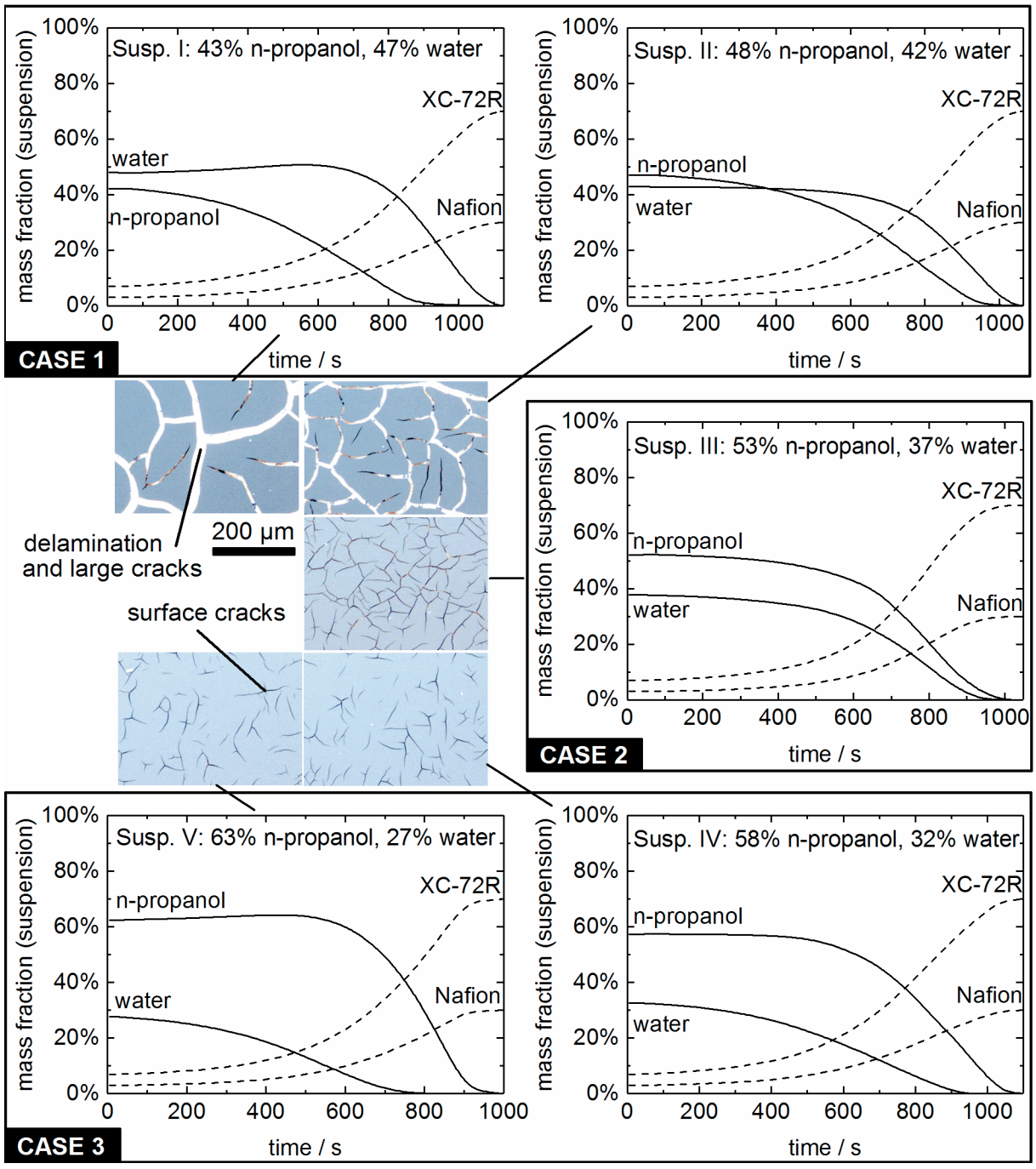

Figure 2. Layer composition as a function of time for the five suspensions listed in Figure 1. The curves relate to the microscopic images (450 x 325 µm²). Two types of cracks are visible: adhesion cracks (white) and surface cracks (black). The gas temperature, as well as the target chamber temperature, was set to T = 40 °C and the layer was overflowed with dry nitrogen (water partial pressure p_w = 0 Pa) at a gas flow velocity of u = 4.4 mm s^{-1}. These parameters are the reference condition of this work. The measurement uncertainties did not exceed 2wt% for a 95% confidence interval.

Variation of Drying Parameters

A way to influence the cracking behavior by adjusting suspension composition was demonstrated above. Unfortunately, chemical and physical properties will be affected, making the unveiling of

structure/dispersion relationships even more complex. At this point, drying kinetics must be used to aid in the preparation of suspension with desired properties. To demonstrate the beneficial effect of drying kinetics, suspension III was dried under various conditions, namely varying temperature, gas velocity and gas moisture. The experiments are listed in Table 1.

Table 1. List of experiments carried out to demonstrate the influence of parameters on the drying process using suspension III. Condition A was the reference condition (see Figure 3). The gas velocity is meant to be the velocity of the nitrogen flow.

Condition	A	B	C	D	E	F	G
Temperature / °C	40	**50**	**60**	40	40	40	40
Gas velocity / mm s^{-1}	4.4	4.4	4.4	**0.9**	**8.8**	4.4	4.4
Humidity / hPa	0	0	0	0	0	**14**	**27**
Total drying time / s	1047	656	512	3772	766	1221	1249

Temperature

In addition to the measuring at the reference target temperature (40 °C, condition A), suspension III was dried at 50 °C (condition B) and 60 °C (condition C); the results are presented in Figure 3. We refrained from carrying out measurements at even higher temperatures, because the film would dry before higher temperatures could be reached. A slight enrichment of n-propanol would be expected when increasing the temperature up to 90 °C due to a stronger increase of the propanol partial pressure for a certain temperature increase compared with the water partial pressure increase; however, the effect on n-propanol concentration is small because the boiling points differ by 2 °C, thus, making it impossible to resolve this in our measurements.

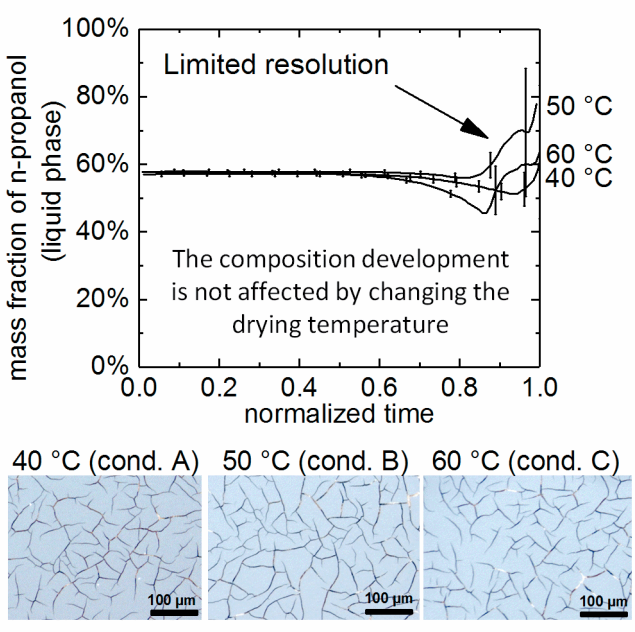

Figure 3. Mass fraction of n-propanol in the liquid phase as a function of normalized times at different conditions (cond.). The drying curves relate to microscopic images (450 x 325 μm^2) of the surfaces. The

deviations between the expected compositions in the remaining 20% of measuring time are statistically insignificant.

The results show that temperature is the simplest way to control the total drying time (see Table 1) without significantly changing the solvent composition. Deviations at the last part of the drying curves are within the increasing measurement uncertainty due to the low residual solvent remained in the almost dried layer (compare reference [39]). Microscopic images showed no differences at increased temperatures, which also confirm the assumption of low effects of the temperature on surface crack formation. If the materials used are stable at a given higher temperature, one should easily use it as a way to efficiently dry the films at a much higher speed.

Gas velocity

When increasing the gas velocity, the concentration in the bulk of the gas-phase is reduced. In consequence, the concentration gradient between gas-side interface and bulk is increased resulting in an increasing diffusive mass transport. By the higher mass transport the gas-side interface solvent concentration is reduced by which the gradient between the gas-side and liquid-side interface increases. This leads to an increasing mass transport through the boundary layer. The effect of increasing mass transport correlates with the gas-side mass transfer coefficient. Therefore, the molecule with a higher gas-side mass transfer coefficient is depleted in the liquid phase. This observation corresponds to earlier publications [21]. An enrichment of n-propanol is expected when doubling the gas velocity from 4.4 to 8.8 mm s^{-1} (condition E). If the gas exchange rate is reduced to 0.9 mm s^{-1} (condition D), the drying time will substantially increase (compare Table 1) while water will be expected to be enriched. The results of the experiments are summarized in Figure 4. As was previously demonstrated, the drying time was normalized to facilitate the interpretation.

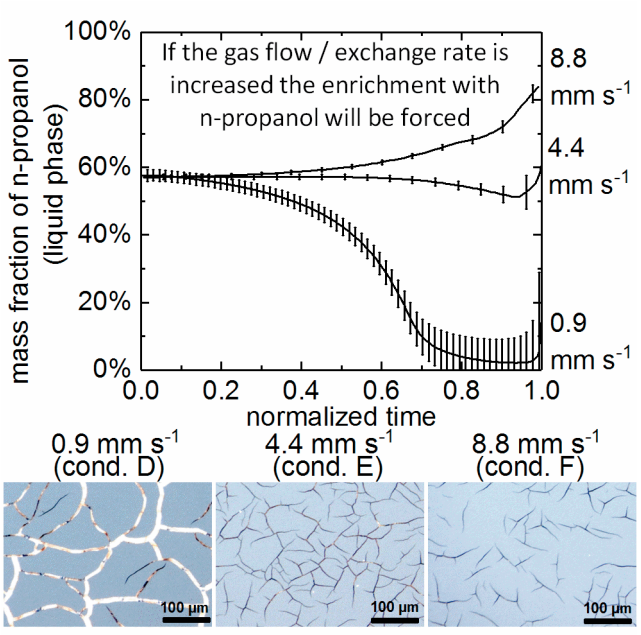

Figure 4. Mass fraction of n-propanol in the liquid phase as a function of normalized time at different gas velocities. The drying curves are related to microscopic images (450 x 325 µm^2) of the surfaces. When

increasing the measuring time and reducing the concentration, the measuring method used become more inaccurate thus leading to larger error bars as can be seen at 0.9 mm s^{-1}.

In the case of low gas velocities, the enrichment of water was confirmed by our measurements. The surface structure was comparable to the layer structure of dispersion II from the last section. In the direction of higher gas velocities compared to the reference, an enrichment of n-propanol appeared. The surface structure is comparable to the dried layer processed from suspension IV and V. These results are of high importance, as control of the layer structure formation by drying kinetics is proven. With the change in the gas velocity, the drying time as well as the selectivity is controllable.

Humidity

It can be assumed that the evaporation rate of a solvent will decrease if the drying gas is preloaded with the same solvent, which eventually leads to enrichment with it [21]. Furthermore; the drying time is expected to increase with higher preloading. In our experiments, the gas phase was pre-humidified with water vapor partial pressures of 13 hPa (condition F, equivalent to 50% relative humidity at 23 °C or 19% relative humidity at 40 °C) and 27 hPa (condition G, equivalent to 95% relative humidity at 23 °C or 36% relative humidity at 40 °C). The results were compared to the reference (see Figure 5). As expected, the drying time increased (see Table 1), and water enrichment could also be confirmed. Concerning the results from the previous subsections, the crack behavior under condition G was, as expected, as the surface tension increased during the drying of the layer. The drying under condition F, however, showed a different crack formation. While most of the cracks were on the surface, only a partial delamination from the substrate is visible. We relate the delamination areas to the higher stress due to the crack geometry at spots where the cracks branch. Moreover, cracks are favored when, locally, water is enriched, which causes a higher local tension. As a result, preloading can be used to influence both the drying time and selectivity of the evaporation.

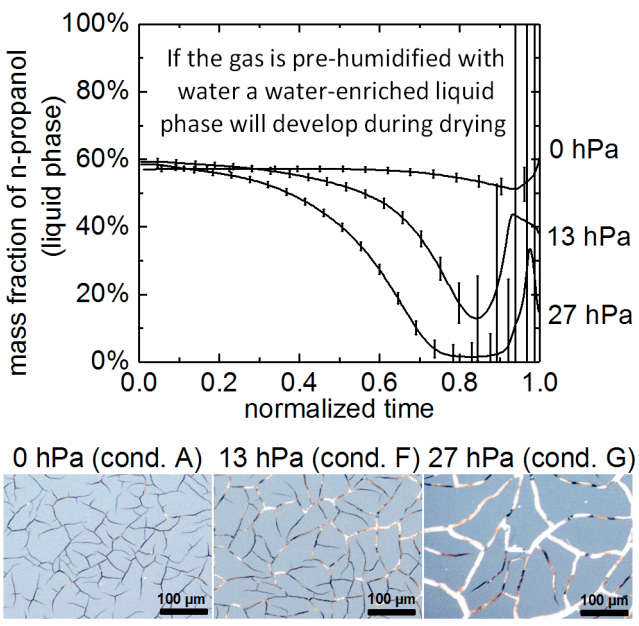

Figure 5. Mass fraction of n-propanol in the liquid phase as a function of normalized time at different water vapor partial pressures. The drying curves are related to microscopic images (450 x 325 μm^2) of the

surfaces. The gas phase was pre-humidified with water vapor partial pressures of 13 hPa (condition F, equivalent to 50% relative humidity at 23 °C or 19% relative humidity at 40 °C) and 27 hPa (condition G, equivalent to 95% relative humidity at 23 °C or 36% relative humidity at 40 °C). The measurement uncertainty is increased by technical implementation of the pre-humidification of the gas phase.

The experiments confirmed our expectations for the combination of the principle of film formation and cracking and the principle of selective drying in multi-solvent systems. These are summarized in Figure 6 for the n-propanol / water system we used for this work. It must be taken into account that the indirectness of the measuring technique did not allow for the collecting of local information about the drying process. Therefore, local drying effects, which result from thickness inhomogeneity and drying front, are invisible in the current state. In addition to that, it must be considered that drying conditions may have an impact on particle movement, particle agglomeration and dry layer thickness, which might affect film formation and crack behavior. However, cross-sectional imaging with the optical microscope did not help in clarification due to its limited resolution. Furthermore, imaging by scanning electron microscopy (compare the right side of Figure 6) is challenging for reasons of polymer destructions / vaporizing.

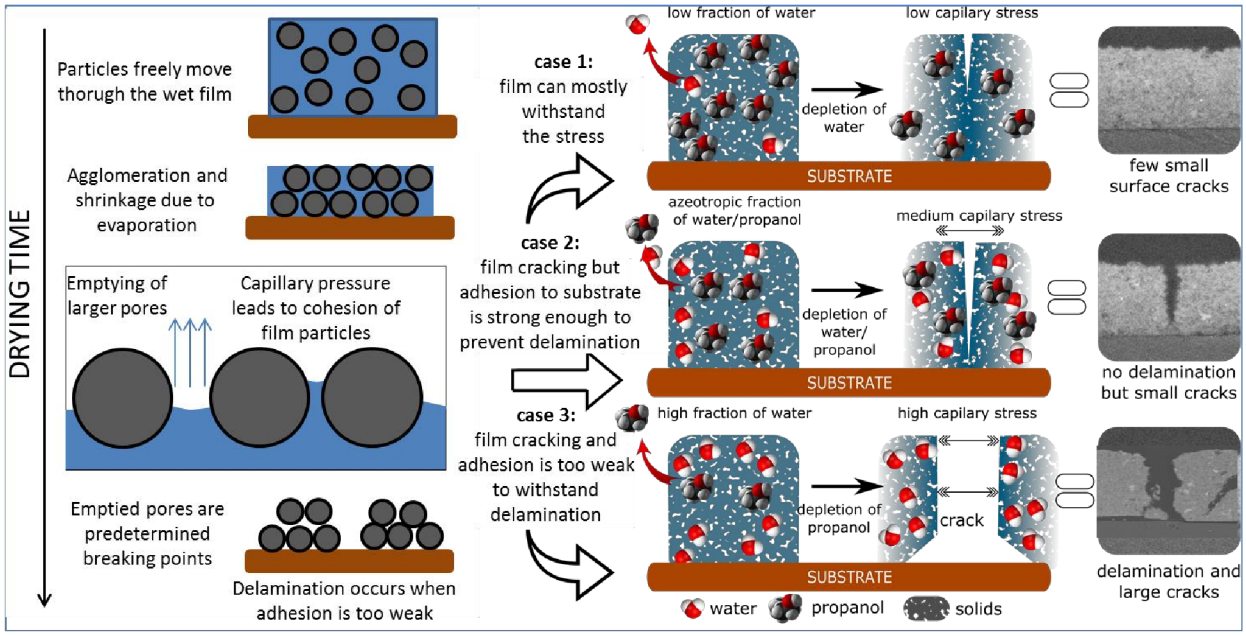

Figure 6. A schematic view of the film formation process during the selective drying. With continuing evaporation of solvent the particles start to agglomerate. Solvent remains in the pores affecting capillary pressure that leads to cohesion of film particles. By the further shrinkage of the film already emptied pores are predetermined breaking points of the film. If the capillary pressure is too high compared with the adhesion between film particles and substrate the film delaminates. The occurrence of cracks and delamination are thus depending on the solvent that is enriched during the drying by which the surface tension of the liquid in the capillaries is increased or decreased.

Conclusion

The preparation of solid-containing suspensions for film manufacture is a common task in a variety of industrial and laboratory applications, including thin film electrodes. Changes that are introduced when making these dispersions will have a variety of unknown positive and negative effects on the final manufactured films, since all parameters and properties of both the suspension and film are fully interdependent. The following insights can be drawn from these findings:

1. Crack formation is correlated with the selective drying of the liquid in the electrode layer, which can be controlled by altering the drying condition.
2. If water is enriched over time during drying, cracks will largely be developed and a delamination from the substrate will occur due to a strong increase in the surface tension and the low surface energy of the substrate.
3. If n-propanol is enriched, the surface tension will decrease, lowering the capillary stress. In this case, only small cracks will develop at the surface of the layer.
4. The temperature does not show a significant influence on drying selectivity; however, the drying time is reduced at higher temperatures and crack formation is unaffected by this.
5. The gas velocity is of major importance, as it controls both the drying time and drying selectivity. High gas exchange numbers result in n-propanol enrichment, while the drying time is reduced. Low velocities, meanwhile, lead to water enrichment and high drying times. The drying-induced cracks are not distinguished from those when the suspension was initially enriched with water.
6. With an increase in the gas vapor partial pressure, the drying is slowed and water is enriched in the liquid phase.

In particular, the development of electrodes for a variety of applications may benefit from key progress in the controlled fabrication of films. Current methods already allow for the fabrication of electrodes with reasonable performance and durability, which in turn can promote their large-scale fabrication. But this is only for a few specific, over-designed fabrication processes. Specific controls over detailed steps during electrode manufacturing have only been modestly demonstrated. In future, we hope to aid scientists in obtaining full control over every single step of electrode manufacturing, so as to maximize the performance and durability of films from the laboratory scale (< 1cm²) to large-scale applications (> 1 m²).

Acknowledgements

The authors acknowledge financial support from the Bavarian Ministry of Economic Affairs and Media, Energy and Technology for the joint projects within the framework of the Helmholtz Institute Erlangen-Nürnberg for Renewable Energy (IEK-11) of Forschungszentrum Jülich.

Reference

1 Kloke, A., von Stetten, F., Zengerle, R., Kerzenmacher, S., “Strategies for the Fabrication of Porous Platinum Electrodes”, Adv. Mater., 23 (43), 4976 (2011), https://doi.org/10.1002/adma.201102182

2 Shimoda, T., Matsuki, Y., Furusawa, M., Aoki, T., Yudasaka, I., Tanaka, H., Iwasawa, H., Wang, D., Miyasaka, M., Takeuchi, Y., “Solution-processed silicon films transistors”, Nat. Lett., 440 (6), 783 (2006), https://doi.org/10.1103/PhysRevLett.98.218302

3 He, B., Yang, S., Qin, Z., Wen, B., Zhang, C., "The roles of wettability and surface tension in droplet formation during inkjet printing", Sci. Report, 7, 11841 (2017), https://doi.org/10.1038/s41598-017-12189-7

4 Lu, Y., Ganguli, R., Drewien, C.A., Anderson, M.T., Brinker, C.J., Gong, W., Guo, Y., Soyez, H., Dunn, B., Huang, M.H., Zink, J.I., "Continuous formation of supported cubic and hexagonal mesoporous films by sol-gel dip-coating", Nature, 389, 364-368 (1997), https://doi.org/10.1103/PhysRevLett.98.218302

5 Jones, D., Vak, D., Weerasinghe, H., Ramamurthy, J., Brown, M., Subbiah, J., "Reverse gravure coating for roll-to-roll production of organic photovoltaics", Sol. Ener. Mater. Sol. Cells, 149, 154-161 (2016), https://doi.org/10.1016/j.solmat.2016.01.015

6 Sandström, A., Dam, H.F., Krebs, F.C., Edman, L., "Ambient fabrication of flexible and large-area organic light-emitting devices using slot-die coating", Nat. Commun., 3, 1002 (2012), https://doi.org/10.1038/ncomms2002

7 Pierre, A., Sadeghi, M., payne, M.M., Facchetti, A., Anthony, J.E., Arias, A.C., "All-Printed Flexible Organic Transistors Enabled by Surface Tension-Guided Blade Coating", Adv. Mater., 26 (32), 5722-5727 (2014), https://doi.org/10.1002/adma.201401520

8 Singh, K.B., Tirumkudulu, M.S., "Cracking in Drying Colloidal Films", Phys. Rev. Lett., 98 (21) 218302 (2007), https://doi.org/10.1103/PhysRevLett.98.218302

9 Ouyang, L., Wei, B., Kuo, C.-C., Pathak, S., Farrell, B., Martin, D.C., „Enhanced PEDOT adhesion on solid substrates with electrografted P(EDOT-NH2)", Sci. Adv., 3 (3), e1600448 (2017), https://doi.org/10.1126/sciadv.1600448

10 Pandey, A., Scheel, J.D., Schumacher, J., "Turbulent superstructures in Rayleigh-Bénard convection", Nat. Commun., 9, 2118 (2018), https://doi.org/10.1038/s41467-018-04478-0

11 Scriven, L.E., Sternling, C.V., "The Marangoni Effects", Nature, 187, 186-188 (1960), https://doi.org/10.1038/187186a0

12 Staehler, M., Friedrich, I., „Statistical Investigations of basis weight and thickness distribution of continuously produced fuel cell electrodes", J. Power Sources, 242, 425-437 (2013), https://doi.org/10.1016/j.jpowsour.2013.05.073

13 Liu, Y., Zhao, J., Li, Z., Mu C., Ma, W., Hu, H., Jiang, K., Lin, H., Ade, H., Yan, H., „Aggregation and morphology control enables cases of high efficiency polymer solar cells", Nat. Commun., 5, 5293 (2014), https://doi.org/10.1038/ncomms6293

14 Oosterhout, S.D, Wienk, M.M., van Bavel, S.S., Thiedmann, R., Koster, L.J.A., Gilot, J., Loos, J., Schmidt, V., Janssen, R.A.L., "The effect of three-dimensional morphology on the efficiency of hybrid polymer solar cells", Adv. Mater., 8 (14-15), 1434-1449 (2009), https://doi.org/10.1002/adma.200802854

15 Peckham, T.J., Holdcraft, S., „Structure-Morphology-Property Relationships of Non-Perfluorinated Proton-Conducting Membranes", Adv. Mater., 22 (42), 4667-4690, (2010), https://doi.org/10.1002/adma.201001164

16 Schaaf, P., Voegel, J.-C., Jierry, L., Boulmedais, F., „Spray-Assisted Polyelectrolyte Multilayer Buildup: from Step-by-Step to Single-Step Polyelectrolyte Film Constructions“, Adv. Mater., 24 (8), 1001-1016 (2010), https://doi.org/10.1002/adma.201001164

17 Schmidt-Hansberg, B., Colsmann, H., Lemmer, U., Schabel, W., „Drying oft thin film polymer solar cells“, European Physical Journal Special Topics, 166, 49, (2009), https://doi.org/10.1140/epjst/e2009-00877-y.

18 Font, F., Protas, B., Richardson, G., Foster, J., „Binder migration during drying of lithium-ion battery electrodes: Modelling and comparison to experiment”, J. Power Sources, 393, 177-185 (2018), https://doi.org/10.1016/j.jpowsour.2018.04.097

19 Calín-Sánchez, A., Kharaghani, A., Lech, K., Figiel, A., Carbonell-Barrachina, AA., Tsotsas, E., “Drying Kinetics and Microstructural and SensoryProperties of Black Chokeberry (Aronia melanocarpa) as Affected by Drying Method”, Food and Bioprocess Technology, 8 (1), 66-74 (2015), https://doi.org/10.1007/s11947-014-1383-x

20 Thurner, F., Schlueder, EU., “Wet-Bulb Temperature of Binary Mixtures”, Chem. Eng. Process., 19, 337-343 (1985), https://doi.org/10.1016/0255-2701(85)85006-6

21 Riede, T., Schluender, E.U., “Selective Evaporation of a Binary Mixture into Dry or Humidified Air”, Chem. Eng. Process., 27 (2) 83-93 (1990), https://doi.org/10.1016/0255-2701(90)85012-S

22 Brown, G.L., “Formation of Films from Polymer Dispersions”, J. Polymer Science, 22 423-434 (1956), https://doi.org/10.1002/pol.1956.1202210208

23 Martinez, CJ., Lewis, JA., “Shape Evolution and Stress Development during Latex Silica Film Formation”, Langmuir, 18, 4689-4698 (2002), DOI: 10.1021/la0114833

24 Price, KK., Wu, Y., McCormick, AV., Francis, LF., “Stress Development in Hard Particle Coatings in the Absence of Lateral Drying”, J. Am. Ceram. Soc., 98 (7), 2214-2222 (2015), https://doi.org/10.1111/jace.13580

25 Tang, CS., Cui, YJ., Tang, AM., Shi, B., “Experiment evidence on the temperature dependence of desiccation cracking behavior of clayey soils”, Engineering Geology, 114 (3-4), 261-266 (2010), https://doi.org/10.1016/j.enggeo.2010.05.003

26 Tirumkudulu, MS., “Cracking in Drying Latex Films”, Langmuir, 21, 4938-4948 (2005), DOI: 10.1021/la048298k

27 Chiu, RC., Cima, MJ., “Drying of Granular Ceramic Films: II, Drying Stress and Saturation Uniformity”, J. Am. Ceram. Soc., 76 (11), 2769-2777 (1993), https://doi.org/10.1111/j.1151-2916.1993.tb04014.x

28 Bauer, C., Cima, M., “Stress Development During Drying of Aqueous Zirconia Based Tape Casting Slurries Measured by Transparent Substrate Deflection Method”, J. Am. Ceram. Soc., 92 (6) 1178-1185 (2009), DOI: 10.1111/j.1551-2916.2009.03000.x

29 Chiu, RC., Garino, TJ., Cima, MJ., "Drying of Granular Ceramic Films: II, Effect of Processing Variables on Cracking Behavior", J. Am. Ceram. Soc., 76 (9), 2257-2264 (1993), https://doi.org/10.1111/j.1151-2916.1993.tb07762.x

30 Xu, P., Mujumdar, AS., Yu, B., "Drying-Induced Cracks in Thin Film Fabrication from Colloidal Dispersions", Drying Technology, 27 (5), 636-652 (2009), DOI: 10.1080/07373930902820804

31 Caddock, BD., Hull, D., "Influence of humidity on the cracking patterns formed during the drying of sol-gel drops", Journal of Material Science, 37 (4), 825-834 (2002), https://doi.org/10.1023/A:1013808402289

32 Tsushima, S., Hirai, S., "An overview of cracks and interfacial voids in membrane electrode assemblies in polymer electrolyte fuel cells", J. Thermal Science and Technology, 10 (1) JTST0002 (2015), https://doi.org/10.1299/jtst.2015jtst0002

33 Komada, Y., Okabayashi, K., Nishimura, H., Hiromitsu, M., Oboshi, T., Usui, H., "Dependence of polymer electrolyte fuel cell performance on preparation conditions of slurry for catalyst layers", J. Power Sources, 193 (2) 488-494 (2009), https://doi.org/10.1016/j.jpowsour.2009.04.015

34 Schonert, M., Jakoby, K., Schluhmbohm, C., Gluesen, A., Mergel, J., Stolten, D., "Manufacture of Robust Catalyst Layers for the DMFC", Fuel Cells, 4 (3) 175-179 (2004), https://doi.org/10.1002/fuce.200400027

35 Dixit, M.B., Harkey, B.A., Shen, F., Hatzell, K.B., "Catalyst Layer Ink Interactions That Affect Coatability", J The Electrochemical Society, 165 (5) 264-271 (2018), https://doi.org/10.1149/2.0191805jes

36 Huang, D.C., Yu, P.J., Liu, F.J., Huang, S.L., Hsueh, K.L., Chen, Y.C., Wu, C.H., Chang, W.C., Tsau, F.H., "Effect of Dispersion Solvent in Catalyst Ink on Proton Exchange Membrane Fuel Cell Performance", Int. J. Electrochem. Sci, 6 (7) 2551-2565 (2011)

37 Scheepers, F., Staehler, A., Staehler, M., Carmo, M., Lehnert, W., Stolten, D., „Layer Formation from Polymer Carbon-Black Dispersions", Coatings, 8 (12), 450, DOI: 10.3390/coatings8120450

38 Burdzik, A., Staehler, M., Friedrich, I., Carmo, M., Stolten, D., "Homogeneity analysis of square meter-sized electrodes for PEM electrolysis and PEM fuel cells", J. Coat. Technol. Res., (2018), https://doi.org/10.1007/s11998-018-0074-3

39 Scheepers, F., Burdzik, A., Staehler, M., Carmo, M., Lehnert, W., Stolten, D., "A New Setup for the Quantitative Analysis of Drying by the use of gas phase FTIR-spectroscopy", Rev. Scientific Instruments 89, 083102 (2018), https://doi.org/10.1063/1.5036817